2008

Formation of Aluminum Hydride during Alkaline Dissolution of Aluminum

Saikat Adhikari
Iowa State University

Jinju Lee
University of Illinois at Urbana-Champaign

Kurt R. Hebert
Iowa State University, krhebert@iastate.edu

Formation of Aluminum Hydride during Alkaline Dissolution of Aluminum

Abstract
The role of hydrogen-containing surface species in the alkaline dissolution of aluminum was studied by secondary ion mass spectrometry (SIMS) and atomic force microscopy (AFM). The measurements revealed quasi-periodic nucleation and dissolution of large number densities of size particles, during open-circuit dissolution in NaOH(D) at room temperature. SIMS results using deuterated solutions, and prior Auger microprobe measurements, indicated that the particles were composed of aluminum hydride (deuteride), with an aluminum hydroxide (deuteroxide) surface layer. The measured open-circuit potential during dissolution was close to the Nernst potential of hydride oxidation. It was concluded that forms continuously during dissolution by reaction of cathodically generated hydrogen with the Al metal and is oxidized to aluminate ions in the accompanying anodic process. The present results are a direct confirmation of hydride formation on Al accompanying corrosion.

Keywords
aluminum compounds, atomic force microscopy, corrosion, dissolving, electrochemistry, nucleation, secondary ion mass spectra, solutions

Disciplines
Chemical Engineering

Comments
This article is from *Journal of the Electrochemical Society* 155 (2008): C16–C21, doi:10.1149/1.2800770. Posted with permission.

Journal of The Electrochemical Society, **155** (1) C16-C21 (2008)
0013-4651/2007/155(1)/C16/6/$23.00 © The Electrochemical Society

Formation of Aluminum Hydride during Alkaline Dissolution of Aluminum

Saikat Adhikari,[a,*] Jinju Lee,[b,c] and Kurt R. Hebert[a,,z]**

[a]*Department of Chemical and Biological Engineering, Iowa State University, Ames, Iowa 50011, USA*
[b]*Center for Microanalysis of Materials, University of Illinois at Urbana-Champaign, Urbana, Illinois 61801, USA*

The role of hydrogen-containing surface species in the alkaline dissolution of aluminum was studied by secondary ion mass spectrometry (SIMS) and atomic force microscopy (AFM). The measurements revealed quasi-periodic nucleation and dissolution of large number densities of 10–100 nm size particles, during open-circuit dissolution in 1 M NaOH(D) at room temperature. SIMS results using deuterated solutions, and prior Auger microprobe measurements, indicated that the particles were composed of aluminum hydride (deuteride), with an aluminum hydroxide (deuteroxide) surface layer. The measured open-circuit potential during dissolution was close to the Nernst potential of hydride oxidation. It was concluded that AlH_3 forms continuously during dissolution by reaction of cathodically generated hydrogen with the Al metal and is oxidized to aluminate ions $[Al(OH)_4^-]$ in the accompanying anodic process. The present results are a direct confirmation of hydride formation on Al accompanying corrosion.
 [DOI: 10.1149/1.2800770]

Manuscript submitted May 29, 2007; revised manuscript received September 6, 2007. Available electronically October 31, 2007.

The electrochemistry of aluminum in alkaline solutions is of technical interest, in part, because of the high voltage and energy density of aluminum-air batteries.[1] Concentrated alkaline solutions are typically used in batteries because of the need for active kinetics, but also present the drawback of metal loss due to corrosion. Many fundamental studies have been carried out on the role of alloying additives that may help control anode activity. Investigations of pure aluminum in alkaline solutions have clarified important aspects of the electrochemical behavior.[2-9] The potential dependence of anodic dissolution was revealed by measurement of the rate of concurrent cathodic hydrogen evolution.[4-7] The formation of aluminum hydroxide or oxide corrosion product films by dissolution has been deduced from studies of anodic kinetics using rotating disk electrodes,[2,6] and from ellipsometry.[3] Impedance studies have revealed complex dynamic behavior, which has been attributed to the contribution of multiple reaction steps to dissolution.[5,9] In all cases, it has been assumed that the overall anode process is simply the oxidation of aluminum metal to aluminate ions. Dissolution occurs at a large surface kinetic overpotential relative to the Nernst potential of this reaction, i.e., ~0.6 V at pH 14.[4,10] This large overpotential has been attributed to a resistive surface film.[2,3,6] It has been shown that the Al dissolution potential corresponds closely to the Nernst potential for oxidation of aluminum hydride to aluminate ions, suggesting the possible function of hydride as a reaction intermediate.[11]

Open-circuit dissolution of Al in alkaline solutions results in substantial rates of hydrogen absorption into the metal,[12-17] as well as the formation of nanoscale voids or hydrogen bubbles in the near-surface region of the metal.[18,19] Understanding of these processes, as they occur in the model system of alkaline dissolution of aluminum, would help elucidate fundamental aspects of the chemical mechanism of hydrogen injection during hydrogen embrittlement. Also, since near-surface voids function as sites for corrosion pits,[20] the formation of these voids is relevant to the mechanism of pit initiation. It has been proposed that both void formation and hydrogen absorption result from injection of hydrogen-vacancy defects during dissolution, which are energetically favored at room temperature due to the large vacancy-hydrogen binding energy in Al.[14,15,19] Therefore, better understanding of the surface chemical processes accompanying dissolution, and in particular, the role of hydrogen, would facilitate explanation of hydrogen absorption and void formation.

Secondary ion mass spectrometry (SIMS) is a highly sensitive surface analytical method that has been used extensively for characterization of H absorption into metals, including Al.[21,22] The present work is a SIMS study of hydrogen absorption into Al during the early stages of alkaline dissolution. We focus on treatment times of a few minutes, which result in activation of the metal surface, and the formation of large quantities of subsurface voids. SIMS was supplemented by atomic force microscopy (AFM), in order to identify surface features correlating with observed transient changes in the SIMS measurements. The results reveal direct evidence for the production of surface hydride species during dissolution of aluminum. Implications for the dissolution mechanism are discussed.

Experimental

The Al samples used for both SIMS and AFM experiments were 110 μm thick foils of 99.99% purity (Toyo). The foil was provided in the as-annealed condition, with typical grain size of 100 μm. In preparation for either experiment, foils were first electropolished in 20% $HClO_4$-ethanol solutions, at 5°C and 30 V, for 5 min. Electropolishing was necessary to obtain a flat reference surface for SIMS, so that the depth of the sputtered crater could be accurately determined. Prior to SIMS, electropolished samples were further treated by open-circuit dissolution in solutions of 1 M NaOD in D_2O, at room temperature. Deuterated baths were used to remove interference from water vapor adsorbed from the atmosphere. Before AFM, the electropolished specimens were prepared by immersion at open circuit in solutions of 1 M NaOH (H_2O) at room temperature. After immersion in the alkaline bath for a selected time, Al samples were removed and washed with deionized H_2O (AFM) or D_2O (SIMS) to quench the reaction.

Time-of-flight (ToF)-SIMS was carried out at the Center for Microanalysis of Materials, University of Illinois at Urbana-Champaign, using a PHI Trift III instrument (Physical Electronics). Four Al foils at a time were placed in the sample holder and mounted in the instrument. The mounting time was ~5 min, and an additional 45 min were required to pump down the vacuum chamber. Because the measurement time was ~30 min per sample, the total transfer time between treatment and measurement for a given foil ranged from 50 to 145 min. The samples were sputtered with a 15 kV Ga^+ beam, and a 2 kV Cs^+ beam was used to analyze negative secondary ions. The sputtered and analyzed areas were 400 × 400 μm and 50 × 50 μm, respectively. During depth profiling, the sample was sputtered for typically 5 s and then analyzed for 8 s. The sputtering rate in the metal was determined to be 0.23 nm/s, by measurement of the depth of a sputtered crater. The sputtering rate in the surface oxide layer was not measured. AFM imaging was carried out in direct contact mode, using a 14 μm scanner with Si cantilevers and a Si_3N_4 tip (Digital Instruments Nanoscope III). The

* Electrochemical Society Student Member.
** Electrochemical Society Active Member.
[c] Present address: Intel Corporation, Santa Clara, California 95052.
[z] E-mail: krhebert@iastate.edu

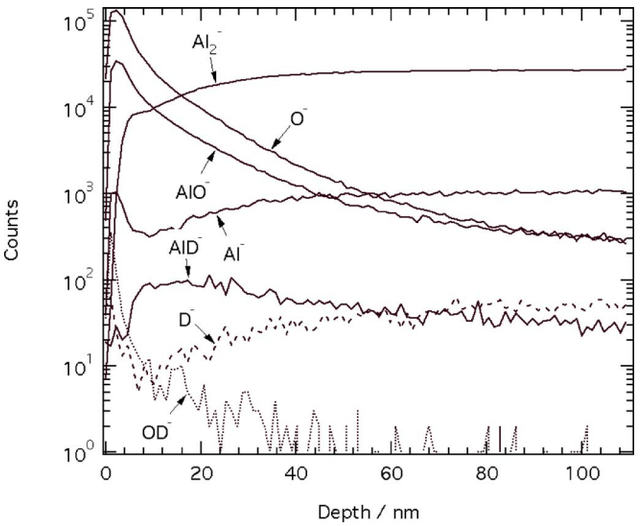

Figure 1. SIMS profiles after caustic dissolution of 99.99% Al for 14.5 min.

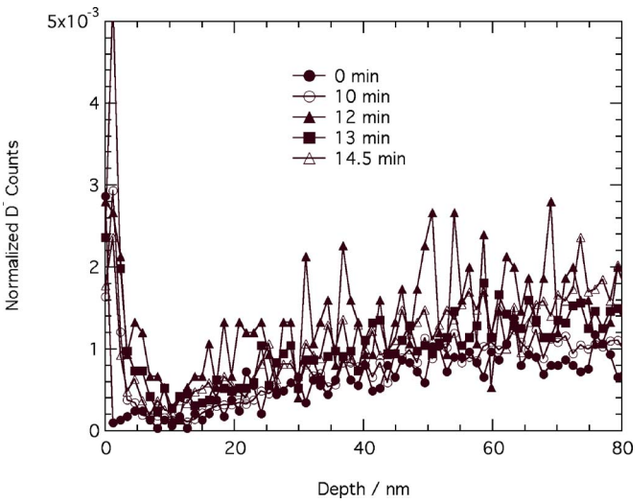

Figure 2. Representative D^- depth profiles after alkaline dissolution of 99.99% Al. Normalization is with respect to bulk Al_2^- counts.

photodiode voltage was set to 4.60 V; assuming a cantilever spring constant of 0.06 N/m, the estimated applied force is 1.5 nN. The scan area was 5 × 5 μm.

Results

Detection of deuterium-containing species with SIMS.— Figure 1 shows a set of depth profiles of negative secondary ions, from a 99.99% Al sample after 14.5 min alkaline dissolution. The profiles of the major negative secondary ions from the oxide film (AlO^-, O^-) and metal (Al^-, Al_2^-) are shown, along with the deuterium-containing species (D^-, AlD^-, OD^-). The peak masses of these species deviated by <0.002 amu from the respective theoretical masses (Table I). The assignment of the 29 amu peak to AlD^-, rather than to a CHO^- fragment possibly derived from sample contamination, is supported by the presence of this peak only in samples exposed to the 1 M NaOD (D_2O) solution, and its strong dependence on dissolution time, as discussed below. OD^- and H_2O^- appeared as separate and readily distinguishable peaks, with the former present only after immersion in the D-containing bath. In Fig. 1, the depth of 5.8 nm corresponds to the decay of the AlO^- peak to half its maximum value, and also to a sharp decrease of slope of the Al_2^- signal. Based on prior work, these features identify this depth as the oxide-metal interface.[23,24] However, the true oxide thickness may not be 5.8 nm because the depth calibration is based on the metal sputtering rate, which generally differs from that in the oxide.

Normalization of the counts of the D-containing species permits comparison of their profiles in samples treated for different times. For this purpose, signals were normalized with respect to the bulk metal level of Al_2^-, which was the dominant peak in the metal in each sample. We made no attempt to determine sensitivity factors of these secondary ions, values of which are needed to compare profiles of different species in terms of concentration. Figure 2 illustrates that the D^- profiles were nearly the same in as-electropolished samples and those treated in NaOD for any time. Because the electropolished samples had not been exposed to deuterium, the measured D^- profiles were evidently due to background contamination rather than alkaline dissolution.

Significant OD^- and AlD^- peaks were not present in mass spectra of as-electropolished samples, but only after treatment in NaOD (D_2O). The OD^- and AlD^- profiles also depended strongly on exposure time to the alkaline bath. Representative depth profiles of OD^- and AlD^- in 99.99% Al are shown in Fig. 3 and 4, for the as-electropolished foil and at dissolution times between 10 and 14.5 min. Both sets of profiles exhibited considerable but nonmonotonic changes with dissolution time. For example, in Fig. 2, the AlD^- profile was flat at 10 min, increased sharply at 12 min, decreased at 13 min, and increased again at 14.5 min. When significant AlD^- was present, the signal was low near the surface, rose to a maximum at 10–20 nm, and then decayed, approaching a constant value at roughly 60 nm. In contrast, the OD^- profiles were confined to depths <4 nm, and did not overlap significantly with the AlD^- profiles.

Table I. Masses of SIMS peaks for D-containing species (for measurements in Fig. 1).

Peak mass (amu)	Assignment	Mass deviation ($\times 10^{-3}$ amu)
2.0141	D^-	0.2
17.9991	OD^-	−0.3
	H_2O	11.4
28.9956	AlD^-	−1.6
	CHO^-	5.5

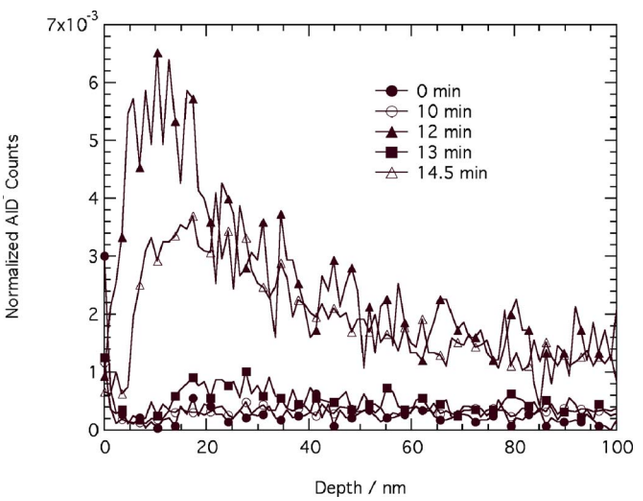

Figure 3. Representative AlD^- depth profiles after alkaline dissolution of 99.99% Al. Normalization is with respect to bulk Al_2^- counts.

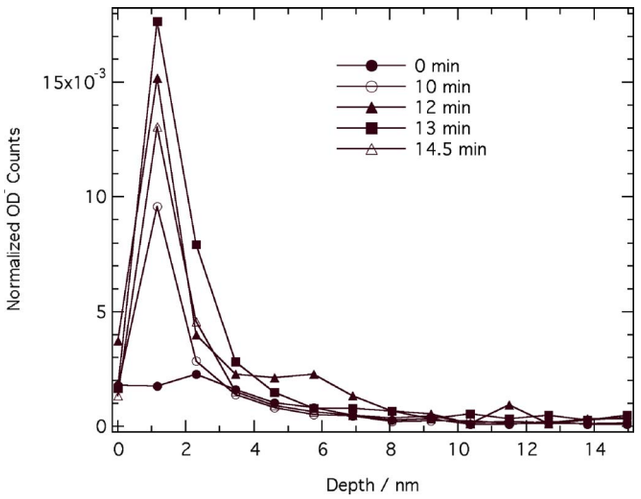

Figure 4. Representative OD^- depth profiles after alkaline dissolution of 99.99% Al. Normalization is with respect to bulk Al_2^- counts.

A large number of dissolution experiments were carried out to characterize the dissolution time dependence of the AlD^- and OD^- profiles. Figures 5 and 6 show the thicknesses and integrated areas of the profiles after different immersion times in NaOD (D_2O). The profile thickness was taken to be the depth at which the mass signal decayed to 1/e, or 36.8%, of its maximum value. Integrated areas were obtained by numerical integration up to depths of 10 nm (OD^-) or 60 nm (AlD^-), after first subtracting the constant background signal approached at large depths. The profile thickness and integrated area were both set to zero when the normalized mass counts did not exceed the background noise level of 0.001 at any depth. According to Fig. 5, significant AlD^- profiles were found only during discrete ranges of dissolution time, during which the AlD^- profile resembled those at 10 and 12 min in Fig. 3. In particular, the AlD^- profile areas and thicknesses rose and fell together, in a series of approximately regular "bursts" at 1, 4, 7–8, and 11–12, and 15 min. The duration of each burst was ~2 min, and bursts were separated by periods of 1–2 min when the AlD^- signal was indistinguishable from background. Figure 6 shows integrated areas

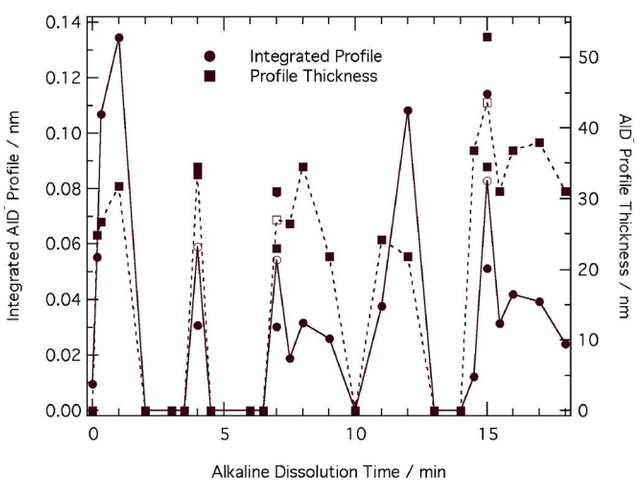

Figure 5. Integrated AlD^- depth profiles and profile thicknesses, after alkaline dissolution of Al samples. The profile thickness is defined as the depth at which the normalized AlD^- counts are a fraction 1/e (i.e., 0.368) of the profile maximum. Open symbols are averages of two data points at the same time.

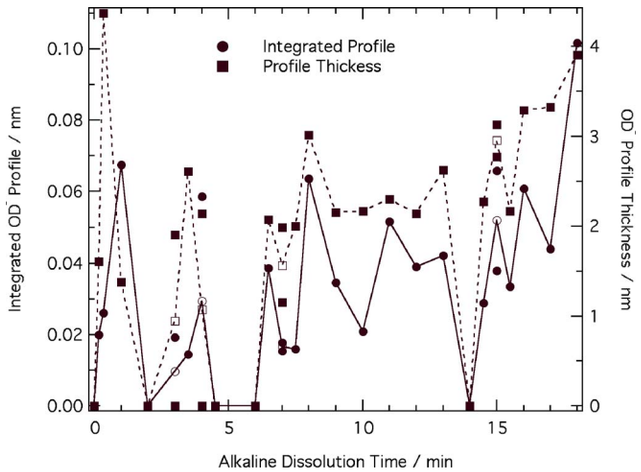

Figure 6. Integrated OD^- depth profiles and profile thicknesses, after alkaline dissolution of Al samples. The profile thickness is defined as the depth at which the normalized OD^- counts are a fraction 1/*e* (i.e., 0.368) of the profile maximum. Open symbols are averages of two data points at the same time.

and depths of the OD^- profiles. Bursts of OD^- were found that coincided with those of AlD^- at 1, 4, and 8 min. However, no further bursts were observed after 8 min, as OD^- profiles were found at all times except 14 min. The measurements after ~7 min suggest the beginning of accumulation of OD^- on the surface.

Surface topography evolution.— The transient bursts of AlD^- and OD^- detected by SIMS may be associated with events in which a new phase nucleates on the Al surface, and then dissolves. For example, the phase might be aluminum deuteroxide because a rotating disk electrode study of Al alkaline dissolution found evidence for a hydroxide film.[2] Evidence for the appearance of a new phase during dissolution was sought through AFM. AFM images were acquired after dissolution of electropolished Al foils in NaOH (H_2O) baths for times up to 10 min. Figure 7 presents examples of such images at times of 40 s, and 1, 2, and 3 min. The typical ridge-scallop topography of the electropolished Al surface is apparent, along with approximately round objects having diameters of <100 nm. These objects are the same as the much less numerous white particles shown clearly in the field-emission scanning electron micrograph of a sample after 4 min dissolution (Fig. 8). The AFM images indicate that the number of particles increased dramatically between 40 s and 1 min, and from 1 and 2 min the particles grew while their number density declined. Both the size and number density decreased significantly from 2 to 3 min. Evidently, particles appeared just prior to 1 min and were removed between 2 and 3 min. These events correspond approximately to the bursts of AlD^- and OD^- detected by SIMS with maxima at 1 min.

Particle size distributions were compiled from the AFM images, in order to quantitatively characterize nucleation, growth, and removal of particles over the same range of times examined by SIMS. Each distribution was obtained using two or three 5×5 μm images from separate experiments at a given dissolution time, and included between 178 and 671 particles. The distributions are plotted in Fig. 9, with the particle numbers in each size category normalized to the same area of 25 μm^2. There were significant increases in particle number density in the intervals 0–1 min and 7–8 min, and another sudden increase may have also occurred between 2–3 min. These times correspond approximately to the bursts of AlD^- detected by SIMS. In each case, the new particles were smaller than 50 nm diam. The distributions at 2 and 9 min contained larger but less numerous particles compared to those at 1 and 8 min, confirming the indication of growth and coalescence in Fig. 7b and c. Then, at

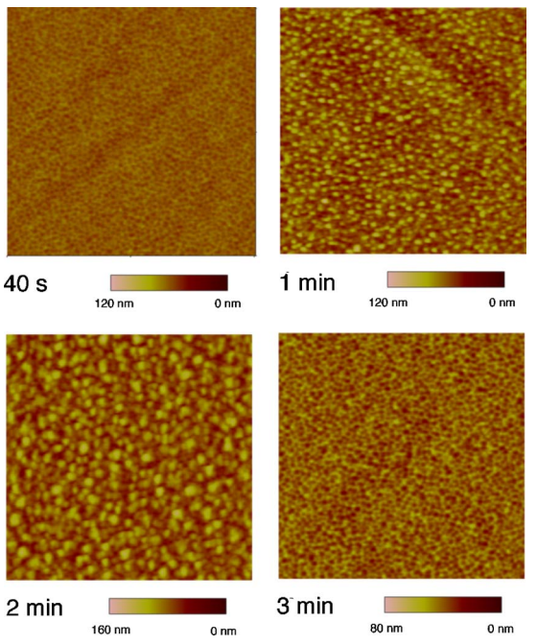

Figure 7. (Color online) Microscopic images of Al surface topography after alkaline dissolution. 5 × 5 μm AFM top view images after 40 s, and 1, 2, and 3 min dissolution, respectively. Conversion of color scale to height is indicated below each image.

3 and 10 min, both the mean particle size and number density decreased. It appears that each particle nucleation event was followed by growth and then by removal, possibly by dissolution. The time elapsed between particle nucleation and removal was ~2 min, similar to the duration of the AlD^- bursts. Therefore, both the timing and duration of the precipitation events are consistent with the AlD^- and OD^- bursts detected by SIMS. Figure 10 shows heights and radii of individual particles, from the distributions at times from 5 to 8 min. At 5, 6, and 7 min, the particle heights were similarly distributed between 5 and 20 min. However, the range of particle heights at 8 min were notably larger, 5–40 nm. Thus, both the number density and average height of particles increased between 7 and 8 min, again corresponding to the rapid elevation of AlD^- and OD^- signals detected by SIMS.

In summary, Fig. 9 reveals small particles on the Al surface irrespective of dissolution time, and in addition relatively large particles at times corresponding to the bursts of AlD^- and OD^-. The small particles may be an artifact of the experimental procedure. That is, upon removal from the alkaline bath, a film of alkaline solution was present on the Al surfaces that would have contained $Al(OH)_4^-$ ions dissolved from the metal. The deionized water used to wash the samples was neutral in pH and may have precipitated these ions as $Al(OH)_3$. This precipitation should have been expected after all dissolution times, but in the SIMS experiments, it would not have contributed to the AlD^- and OD^- signals. Because the dissolution bath was the only source of deuterium, the correlation between the times of the AlD^-/OD^- bursts and large particle nucleation indicates that these particles were formed during alkaline dissolution itself. In addition, there is good agreement between the heights of the large particles (Fig. 10) and the depth of AlD^- profiles (Fig. 5), each of which are ~30 nm. Although this comparison is not quantitatively

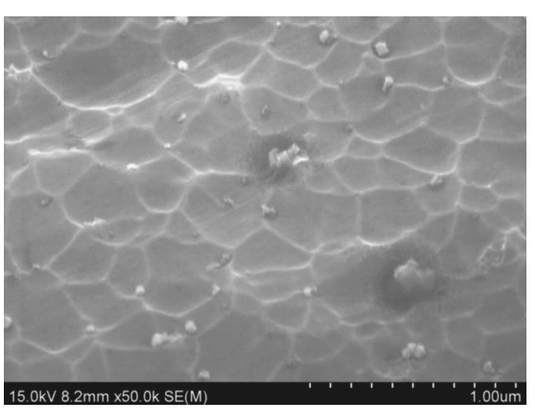

Figure 8. FE-SEM image of Al surface after 4 min alkaline dissolution (image dimensions are 2.5 × 1.7 μm). The sample was dipped in 1 M HNO_3 solution after alkaline treatment.

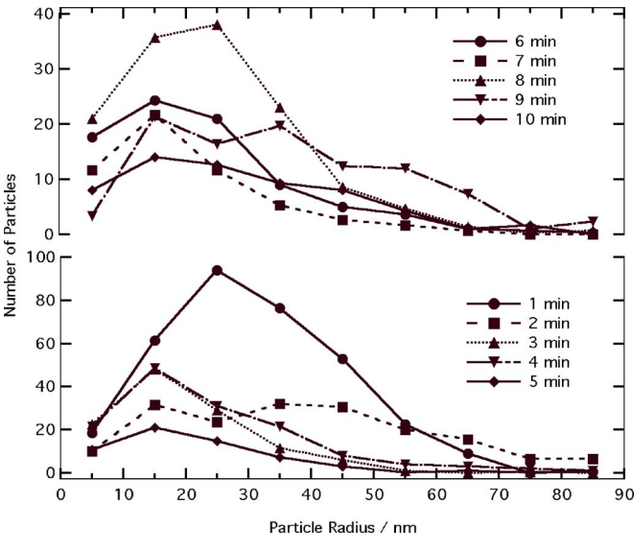

Figure 9. Particle size distributions at various dissolution times, obtained by analysis of AFM images. Particle radius is defined according to $\sqrt{(\text{area})/\pi}$. Number of particles in each size category is referenced to an Al surface area of 25 μm^2.

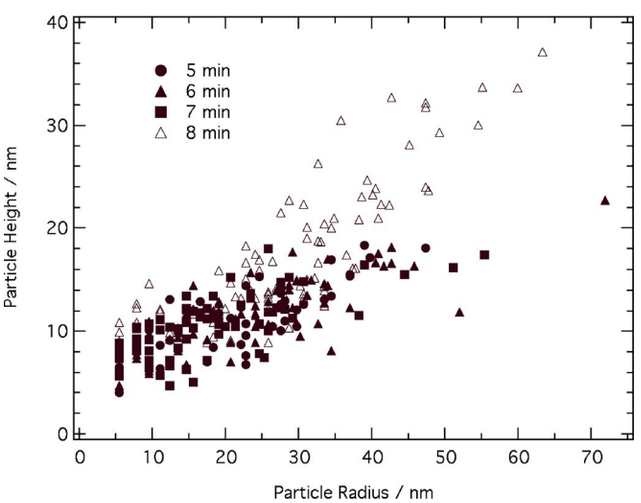

Figure 10. Heights and radii of individual particles, measured by AFM after dissolution times from 5 to 8 min.

rigorous, due to the unknown sputtering rate in the particles, it supports the attribution of AlD^-/OD^- bursts to particle nucleation and removal.

Discussion

The identities of chemical species associated with the OD^-, AlD^-, and D^- peaks are now considered. SIMS spectral peaks for OD^- secondary ions have been found to originate from passive films on Al containing deuteroxyl groups.[24] Although no reports of peaks for the secondary anions AlD^- or D^- were found in the literature, cations such as AlH^+, AlH_2^+, and AlH_3^+ have been detected upon exposing clean Al surfaces to hydrogen.[25-30] These cations have been shown to result from aluminum hydride species (AlH_3, Al_3H_6) formed by the chemical reaction of Al with hydrogen. Based on these comparisons to the literature, the AlD^- peak is not due to deuteroxyl groups in the surface film and is more likely attributable to an aluminum deuteride surface species. As noted above, the timing of the AlD^- bursts corresponds to the appearance of particles in AFM images, and the particle heights agree with the depth of the AlD^- profiles. Therefore, because AlD^- cannot be assigned to a deuteroxide phase, we conclude that the particles in AFM were composed primarily of an aluminum hydride corrosion product. Similar AlD_3 particles would have been formed in the SIMS experiments. The OD^- bursts coinciding with those of AlD^- are associated with films of several nanometers thickness, occupying the surfaces of these particles. These $Al(OD)_3$ containing films may have formed by oxidation of the deuteride, either in solution or in air following removal from the dissolution bath. The formation of $Al(OD)_3$ by reaction of AlD_3 explains why the AlD^- and OD^- depth profiles did not overlap appreciably (Fig. 3 and 4). Surface oxide films on AlH_3 particles have been noted previously and invoked to explain the stability of the particles.[31]

Support for the proposed assignment of the particles to a hydride (deuteride) phase can be found in earlier field emission scanning Auger microprobe (FE-SAM) measurements, by one of the present authors.[32] Spectra on particles formed by dissolution of 99.99% purity Al foils in 1 M NaOH (H_2O) were acquired, before and after sputtering to depths of 5 and 10 nm, and were compared to those on nearby sites with no particles. An oxide or hydroxide layer of several nanometers' thickness was detected on the particles, but spectra after 10 nm etching were the same as those at equivalent depths on sites away from particles. Because the depth of 10 nm is much greater than the 3 nm oxide thickness on Al metal, it was concluded that particle interiors did not contain appreciable oxygen and were therefore metallic. However, the results can also be explained by AlH_3 particles with surface oxide layers, as hydrogen would not be detectable in Auger spectra, and the electron beam can decompose AlH_3 nanoparticles to metallic Al.[33] Thus, the Auger measurements agree with the identification of the particles as aluminum hydride formed by dissolution.

Prior electrochemical experiments yield further indications that hydride participates in Al dissolution. Perrault showed that the pH dependence of the open circuit potential of cathodically charged Al specimens was quantitatively consistent with equilibria of reactions involving hydride species.[11] In strongly alkaline solutions, he found that the open-circuit potential was determined by the equilibrium of the reaction

$$AlH_3 + 7OH^-(aq) \rightarrow Al(OH)_4^- + 3H_2O(aq) + 6e^- \quad [1]$$

The standard chemical potential of AlH_3 derived from his data was in reasonable agreement with the value from thermochemical measurements.[34] The corresponding Nernst potentials of Reaction 1 at pH 14 are −1.95 and −1.85 V vs Ag/AgCl, respectively. Both values are close to the measured potential in the present experiments, during the first 10 min of dissolution (Fig. 11). In contrast, the Nernst potential of direct Al dissolution at pH 14, −2.56 V vs Ag/AgCl,[10] suggests a large dissolution overpotential and, hence, the presence of a resistive surface layer. Additional indications of hydride were found by Despic et al.[35] and Radosevic et al.,[36] who observed that polarization of Al at cathodic potentials produced an oxidizable substance, which they identified as aluminum hydride, on the basis of its observed oxidation potential.

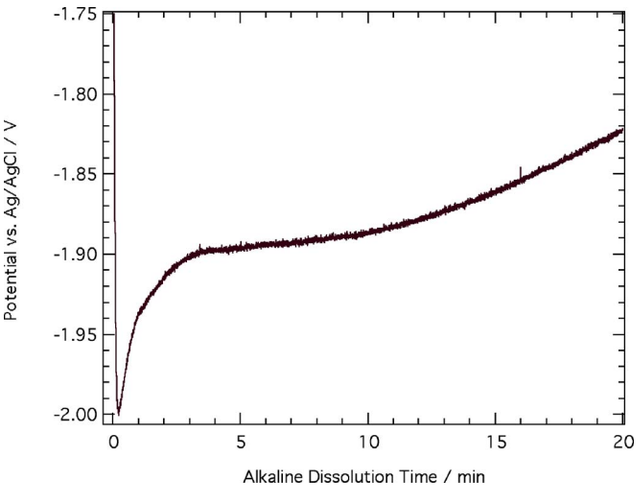

Figure 11. Open-circuit potential during aluminum dissolution in 1 M NaOH (H_2O).

The presence of hydride on the dissolving surface leads us to propose a reaction scheme for open circuit alkaline dissolution of Al. The anodic dissolution Reaction 1 would be accompanied by cathodic reduction of water to form hydrogen

$$H_2O + e^- \rightarrow OH^- + H \quad [2]$$

and the H-induced etching of aluminum to form hydride, as has been extensively observed in vacuum experiments[25-30]

$$Al + 3H \rightarrow AlH_3 \quad [3]$$

The overall dissolution reaction is then

$$2Al + OH^- + 3H_2O \rightarrow Al(OH)_4^- + AlH_3 \quad [4]$$

Thus, the balance of electrons between anodic and cathodic reaction dictates that both aluminate ions and hydride are formed continuously as products of dissolution.

The hypothesis of a reaction pathway involving hydride should be reconciled with earlier indications of precipitated hydroxide films produced by dissolution. Measurements of the rate of decrease of sample thickness, over somewhat longer dissolution times than in the present work, indicated that the corrosion rate was approximately constant at 2 nm/s. Thus, the $Al(OH)_4^-$ concentration near the metal would be expected to increase with time until the solubility of $Al(OH)_3$ is reached. The time of hydroxide precipitation t_p can be estimated using Sand's equation

$$t_p = \pi D \left(\frac{C_s \Omega_{Al}}{v_d} \right)^2 \quad [5]$$

where D is the diffusion coefficient of $Al(OH)_4^-$ ions, C_s is the concentration of $Al(OH)_4^-$ ions at the metal surface when precipitation occurs, Ω_{Al} is the molar volume of aluminum (10 cm^3/mol), and v_d is the dissolution velocity.[37] The diffusion coefficient of $Al(OH)_4^-$ was reported to be 8.4×10^{-6} cm^2/s.[2] C_s was taken as 0.05 M, the solubility of gibbsite, the least soluble form of $Al(OH)_3$ and normally the first precipitate from aqueous solution.[38,39] This value represents a lower bound, because, in general, supersaturation is required for nucleation to occur. With these values, Eq. 5 indicates that t_p is at least 3 min, greater than the time of 1 min when particles first appeared but less than the time of ~7 min when the accumulation of $Al(OH)_3$ was evident in the SIMS measurements (Fig. 6).

Although this calculation is imprecise because the dissolution rate at early times is not known accurately, it further supports the proposal that the particles are not $Al(OH)_3$. At present, we cannot offer an explanation for the observed quasi-periodic bursts of particle formation/dissolution, which appear to occur coherently across the entire Al surface. The absence of potential fluctuations during the bursts (Fig. 11) suggests that they are instead driven by oscillations of the concentration adjacent to the surface.

The absence of significant D^- in the SIMS measurements should be explained because previous SIMS studies of Al after alkaline dissolution or cathodic charging reported profiles of H (D) in the metal as H^- or D^- secondary ions.[21,22] For example, Rozenak et al. exposed Al to NaOD (D_2O) solution for 2 h, and found D^- profiles to depths of ~ 1 μm.[22] If it is assumed that D^- represents a mobile form of deuterium in Al, this apparent discrepancy may be explained by considering diffusion in the metal after the alkaline treatment. The penetration distance of diffusing D into the metal increases with time according to $\delta_D \sim (D_D t)^{1/2}$, where D_D is the interstitial deuterium diffusivity. The present samples were exposed to the alkaline bath for <20 min, and the total transfer time between treatment and measurement was 50–145 min. Because the treatment time was much smaller than the transfer time, any near-surface D absorbed during dissolution would have dispersed from the near-surface region, by diffusion toward the bulk metal. In the experiments of Rozenak et al.,[22] it is likely that the treatment time far exceeded the transfer time, and therefore diffusion during transfer would not have eliminated the D^- profiles. That is, measurement of profiles due to mobile D would require small transfer times relative to the treatment time, a condition which was not met in the present experiments.

Conclusion

The experiments reported here demonstrated that, during open-circuit dissolution of aluminum in 1 M NaOH(D), large number densities of submicrometer particles spontaneously appeared on the surface and then dissolved, at roughly periodic intervals of 3 min. The present SIMS and prior Auger microprobe measurements indicate that the particles are composed of aluminum hydride (deuteride) and are covered with a hydroxide (deuteroxide) film.[32] From a thermodynamic point of view, the formation of hydride can be explained by the close proximity of the dissolution potential to the Nernst potential for the oxidation of hydride to hydroxide. The present results therefore indicate that alkaline dissolution of Al occurs by the continuous anodic oxidation of hydride formed by the accompanying cathodic reaction. It is plausible that hydride forms by reaction of cathodically generated hydrogen with the aluminum substrate, a process which has been found to occur during hydrogen exposure of Al surfaces in vacuum. Aluminum corrosion mechanisms involving hydride have been proposed previously, but the present study is the first analytical detection of hydride formed by dissolution. Continuous hydride formation and oxidation, near the Nernst potential for the latter reaction, suggests that the dissolving aluminum metal surface is not covered by a resistive oxide, as previously considered. Instead, it may be covered by a hydride layer, which prevents oxidation of surface Al atoms. Also, the direct participation of hydrogen in the dissolution reaction provides a possible avenue by which hydrogen-vacancy defects can be continuously formed and may help explain the observed high rates of hydrogen absorption and void formation during dissolution.

Acknowledgments

Financial support was provided by St. Jude Medical Corp., and by the National Science Foundation through grant no. NSF-DMR-0605957. The SIMS measurements were initiated with the invaluable assistance of the late Howard Birnbaum.

Iowa State University assisted in meeting the publication costs of this article.

References

1. Q. F. Li and N. J. Bjerrum, *J. Power Sources*, **110**, 1 (2002).
2. K. E. Heusler and W. Allgaier, *Werkst. Korros.*, **22**, 297 (1971).
3. R. Greef and C. F. W. Norman, *J. Electrochem. Soc.*, **132**, 2362 (1985).
4. O. R. Brown and J. S. Whitley, *Electrochim. Acta*, **32**, 545 (1987).
5. D. D. Macdonald, S. Real, S. I. Smedley, and M. Urquidi-Macdonald, *J. Electrochem. Soc.*, **135**, 2410 (1988).
6. D. Chu and R. F. Savinell, *Electrochim. Acta*, **36**, 1631 (1991).
7. M. L. Doche, J. J. Rameau, R. Durand, and F. Novel-Cattin, *Corros. Sci.*, **41**, 805 (1999).
8. S. I. Pyun and S. M. Moon, *J. Solid State Electrochem.*, **4**, 267 (2000).
9. H. B. Shao, J. M. Wang, Z. Zhang, J. Q. Zhang, and C. N. Cao, *J. Electroanal. Chem.*, **549**, 145 (2003).
10. M. Pourbaix, *Atlas of Electrochemical Equilibria in Aqueous Solutions*, p. 168, Pergamon, New York (1966).
11. G. G. Perrault, *J. Electrochem. Soc.*, **126**, 199 (1979).
12. A. I. Onuchukwu and S. Trasatti, *Electrochim. Acta*, **33**, 1425 (1988).
13. A. I. Onuchukwu, S. P. Trasatti, and S. Trasatti, *Corros. Sci.*, **36**, 1815 (1994).
14. H. K. Birnbaum, C. Buckley, F. Zeides, E. Sirois, P. Rozenak, S. Spooner, and J. S. Lin, *J. Alloys Compd.*, **253**, 260 (1997).
15. C. E. Buckley and H. K. Birnbaum, *J. Alloys Compd.*, **330**, 649 (2002).
16. M. J. Danielson, *Corros. Sci.*, **44**, 829 (2002).
17. E. Lunarska and O. Chernyayeva, *Int. J. Hydrogen Energy*, **31**, 285 (2006).
18. K. R. Hebert, H. Q. Wu, T. Gessmann, and K. Lynn, *J. Electrochem. Soc.*, **148**, B92 (2001).
19. C. E. Buckley, H. K. Birnbaum, J. S. Lin, S. Spooner, D. Bellmann, P. Staron, T. J. Udovic, and E. Hollar, *J. Appl. Crystallogr.*, **34**, 119 (2001).
20. K. Muthukrishnan, K. R. Hebert, and T. Makino, *J. Electrochem. Soc.*, **151**, B340 (2004).
21. G. A. Young and J. R. Scully, in *Hydrogen Effects on Material Behavior and Corrosion Deformation Interaction*, N. R. Moody, Editor, p. 893, Minerals, Metals & Materials Science, Warrendale, PA (2003).
22. P. Rozenak, E. Sirois, B. Ladna, H. K. Birnbaum, and S. Spooner, *J. Alloys Compd.*, **387**, 201 (2005).
23. J. I. Eldridge, R. J. Hussey, D. F. Mitchell, and M. J. Graham, *Oxid. Met.*, **30**, 301 (1988).
24. B. C. Bunker, G. C. Nelson, K. R. Zavadil, J. C. Barbour, F. D. Wall, J. P. Sullivan, C. F. Windisch, M. H. Engelhardt, and D. R. Baer, *J. Phys. Chem. B*, **106**, 4705 (2002).
25. M. Hara, K. Domen, T. Onishi, and H. Nozoye, *Appl. Phys. Lett.*, **59**, 1793 (1991).
26. M. Hara, K. Domen, T. Onishi, and H. Nozoye, *J. Phys. Chem.*, **95**, 6 (1991).
27. M. Hara, K. Domen, T. Onishi, H. Nozoye, C. Nishihara, Y. Kaise, and H. Shindo, *Surf. Sci.*, **242**, 459 (1991).
28. A. Winkler, C. Resch, and K. D. Rendulic, *J. Chem. Phys.*, **95**, 7682 (1991).
29. E. L. Crane and R. G. Nuzzo, *J. Phys. Chem. B*, **105**, 3052 (2001).
30. E. P. Go, K. Thuermer, and J. E. Reutt-Robey, *Surf. Sci.*, **437**, 377 (1999).
31. J. Graetz and J. J. Reilly, *J. Phys. Chem. B*, **109**, 22181 (2005).
32. T. Martin and K. R. Hebert, *J. Electrochem. Soc.*, **148**, B101 (2001).
33. P. J. Herley, W. Jones, and G. R. Millward, *Mater. Lett.*, **7**, 441 (1989).
34. G. C. Sinke, L. C. Walker, F. L. Oetting, and D. R. Stull, *J. Chem. Phys.*, **47**, 2759 (1967).
35. A. R. Despic, D. M. Drazic, J. Balaksina, L. Gajickrstajic, and R. M. Stevanovic, *Electrochim. Acta*, **35**, 1747 (1990).
36. J. Radosevic, M. Kliskic, P. Dabic, R. Stevanovic, and A. Despic, *J. Electroanal. Chem. Interfacial Electrochem.*, **277**, 105 (1990).
37. A. J. Bard and L. R. Faulkner, *Electrochemical Methods: Fundamentals and Applications*, Wiley, New York (2001).
38. W. Feitknecht and P. Schindler, *Pure Appl. Chem.*, **6**, 130 (1963).
39. R. S. Alwitt, in *Oxides Oxide Films*, J. W. V. Diggle, Editor, p. 169, Dekker, New York (1976).